



Article

Wave Climate Variability along the Coastlines of Senegal over the Last Four Decades

Marcellin Seujip Samou ^{1,2,*} , Xavier Bertin ^{2,*}, Issa Sakho ^{3,4} , Alban Lazar ⁵, Mamadou Sadio ⁶ and Mouhamadou Bachir Diouf ¹

¹ Laboratoire de Sédimentologie et de Biostratigraphie, Faculté des Sciences et Techniques, Université Cheikh Anta DIOP de Dakar, Fann, Dakar BP 5005, Senegal; mouhamadou.diouf@ucad.edu.sn

² UMR 7266 Littoral Environnement et Sociétés (LIENSs), CNRS—La Rochelle Université, 2 rue Olympe de Gouges, 17000 La Rochelle, France

³ Université Amadou Mahtar MBOW de Dakar à Diamniadio, UMR Sciences, Technologies Avancées et Développement Durable, Dakar BP 45927, Senegal; issa.sakho@uam.edu.sn

⁴ Université de Rouen Normandie, UNICAEN, CNRS, M2C UMR 6143, 76000 Rouen, France

⁵ UMR 7159 Laboratoire d'Océanographie et du Climat, Expérimentations et Approches Numériques (LOCEAN), La Sorbonne Université, 4 Place Jussieu, 75005 Paris, France; alban.lazar@laposte.net

⁶ Gestion Intégrée et Développement Durable du Littoral Ouest-Africain (GIDEL), Université Cheikh Anta DIOP de Dakar, Fann, Dakar BP 5005, Senegal; sadiomamadou@yahoo.fr

* Correspondence: marcellin.samou_seujip@univ-lr.fr (M.S.S.); xavier.bertin@univ-lr.fr (X.B.)

Abstract: Knowledge of wave climate is essential for efficient management of the world's coastal areas. Senegal is a relevant case, given its high coastal vulnerability to energetic wave conditions. This study investigates wave climates along the coastal zone of Senegal based on a new high-resolution hindcast covering the period 1980–2021. This study evaluates the average, seasonal, and extreme values for the significant wave heights (Hs), periods (T_{m02}/T_p), and mean directions (DIR). In boreal winter, the wave climate is dominated by swells coming from the North-Atlantic lows. In contrast, in boreal summer, the Southern Coast (from Dakar to Casamance) is exposed to swells generated in the South Atlantic Ocean. Throughout their refraction around the Dakar Peninsula, NW swells rotate by $\sim 100^\circ$ from NW to SW, while their Hs is roughly halved when reaching the Southern Coast of Senegal. Over the studied period, trends in Hs are weak (~ 0.6 cm.decade⁻¹) on the Northern Coast and double on the Southern Coast (~ 1.2 cm.decade⁻¹), mostly due to an increase during boreal summer (2 cm.decade⁻¹). The wave periods show weak trends (~ 0.05 s.decade⁻¹), and DIRs show weak counterclockwise rotation (-1° .decade⁻¹). These trends are explained by the main climate modes of the Atlantic Ocean (NAO/EA during winter, SAM during summer) and are important for future research and long-term monitoring of the Senegalese Coast.

Keywords: wave climate; WaveWatch III; wave climatology; wave trends; remote climatic modes; in situ data; Atlantic Ocean; Senegalese Coast; Senegal



Citation: Samou, M.S.; Bertin, X.; Sakho, I.; Lazar, A.; Sadio, M.; Diouf, M.B. Wave Climate Variability along the Coastlines of Senegal over the Last Four Decades. *Atmosphere* **2023**, *14*, 1142. <https://doi.org/10.3390/atmos14071142>

Academic Editors: Mohammad Nabi Allahdadi, Felix Jose and Saeed Shaeri

Received: 24 May 2023

Revised: 6 July 2023

Accepted: 10 July 2023

Published: 13 July 2023



Copyright: © 2023 by the authors. Licensee MDPI, Basel, Switzerland. This article is an open access article distributed under the terms and conditions of the Creative Commons Attribution (CC BY) license (<https://creativecommons.org/licenses/by/4.0/>).

1. Introduction

As the true lung of the world economy, coastal zones are subjected to the perpetual action of ocean short waves (hereafter simply waves), which continuously shape their morphology and may even drive irreversible damages and changes under extreme conditions, impacting coastal ecosystems, infrastructures, socio-economic activities and the safety of human life [1–6]. Research focusing on wave climatology remains rare in the tropical Atlantic, particularly in Western Africa [4,7]. Yet, a good knowledge of wave climate is crucial for decision-making and to reach resilient and sustainable coastal management, particularly in the context of increased coastal risk related to climate change [5,6,8–11]. The increase in significant wave heights (hereafter, Hs) since the second half of the 20th century, as well as changes in other wave parameters (mean periods (T_{m02}) with peaks (T_p) and directions (DIR)) reported at high and medium latitudes north (e.g., [12–14]) and south [15,16], raises

questions about the situation for Senegal. More locally, Dahunsi et al. [17] reported an increase in the extreme values of Hs (99th percentile) and the mean wave period (T_{m02}) in the southern part of the West African coast (Gulf of Guinea, hereafter GG). This was based on retrospective (1979–2005) and prospective (2026–2045 and 2081–2100) wave analysis. Earlier in the same area, based on a 37-year (1980–2016) wave hindcast, Osinowo et al. [18] showed a positive trend in the 99th percentile of Hs, which increases rapidly in GG from East to West (from $0.01 \text{ m.decade}^{-1}$ to $0.3 \text{ m.decade}^{-1}$). Osinowo et al. [18] expect an increase in storms in the western part of the GG. Although located outside of GG, this increase could reach Senegal because its coastline on the Horn of Africa constitutes the extremity of West Africa. However, the long-term trends in wave parameters remain unknown. Other global wave climate analyses based on satellite altimetry found non-significant trends in this region of the tropical Atlantic [19,20]. Nonetheless, these two studies do not cover the same period as Osinowo et al. [18] and Dahunsi et al. [17]. To understand the spatio-temporal variability of waves, many studies have investigated connections/tele-connections between climatic modes (e.g., [12,21–25]) and wave parameters. The wave climate variability in the Atlantic Ocean has been explained by the North Atlantic Oscillation (NAO) [12,14,26–33], the main mode of mid-latitude climate variability in the Northern Hemisphere. Additionally, the Southern Annular Mode (SAM) [15,16,34–37], the main mode of mid-latitude variability in the Southern Hemisphere, has also been linked to wave climate variability. Although little investigated, other modes were shown to explain one part of wave climate variability in the eastern tropical Atlantic [31–33,38–41]. In the GG, Almar et al. [42] found correlations between the SAM index and the wave parameters capable of partly explaining their variability.

Along the Senegalese Coast, only a few studies addressed wave climates [4,7,11]. Based on Era-Interim reanalysis [43] from 1979–2016, Almar et al. [7] established significant correlations between major Atlantic climatic modes and wave variability. These authors found for Hs a strong correlation with NAO in boreal winter and a positive correlation with positive phases of SAM during boreal summer. These authors also related the significant difference between the daily wave activity along the Senegalese Coast and the variability of surface winds from the tropical Atlantic in the boreal summer [7]. Important wave variability and storm events can also occur during transitional seasons (spring and autumn) offshore the Senegalese Coast due to local wind variability, as initially reported by Winant et al. [44] and later supported by Sadio et al. [4] and Colosi et al. [45]. However, these studies rely on extractions of wave parameters from global hindcasts, with resolutions ranging from $0.30^\circ \times 0.30^\circ$ to $0.5^\circ \times 0.5^\circ$, which is way too coarse to represent topographic features, e.g., the Dakar Peninsula, of key importance for wave propagation along the coast. Indeed, the Dakar Peninsula provides shelter for the Southern Coast from Northern swells and for the Northern Coast from swells coming from the south (Figure 1).

To address these limitations and extend this analysis to other parameters such as wave period and directions, this study presents a high-resolution wave hindcast for the Senegalese Coast, which encompasses the period 1980–2021. Based on this hindcast, the local wave climate is described, long-term trends are investigated, and the control of large-scale climatic modes is explored. The following section presents the study area, while Section 3 describes the model and data used for this hindcast. Section 4 describes the wave climate and long-term trends along the coasts of Senegal, while Section 5 investigates the origin of its variability and the link with the main climatic modes. Finally, Section 6 discusses the main findings of this research and their potential implications for the Senegalese Coast.

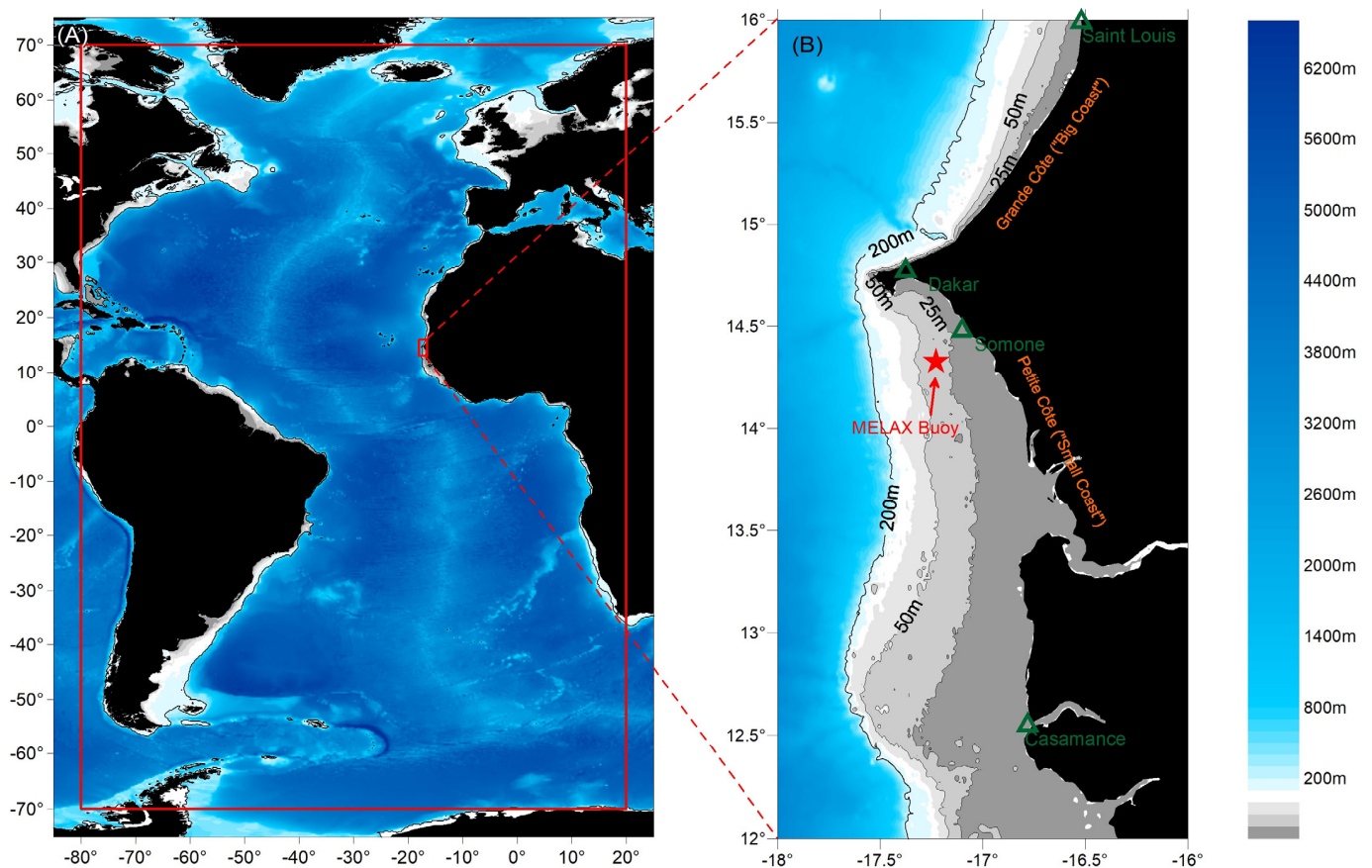


Figure 1. Atlantic Ocean Bathymetry with (A) the extension of the regional domain grid (red rectangle) and (B) the extension of the local grid on the Senegal Coast where the MELAX Buoy is referenced (red star) off Somone on the Petite Côte of Senegal.

2. Study Area

2.1. General Description

Situated to the north of West Africa in the tropical Atlantic (Figure 1A), the Senegalese Coastline (Figure 1B) is home to more than 50% of the country's population and approximately 85% of its industries and services, as well as two of its key economic sectors: fishing and tourism. Established on approximately 700 km long [46], this coastline is essentially characterized by three (3) types of coasts: sandy coasts (the most important), rocky coasts, and muddy coasts with mangroves, of which the most important are located in the Sine-Saloum delta, in Casamance, and along the estuaries of Senegal. This coastal area is divided into two sectors, namely the "Grande Côte" (hereafter Big coast), which goes from the Senegal River mouth (Saint-Louis) to the Cap Verde Peninsula (Dakar), and the "Petite Côte" (hereafter Small coast), which extends from Dakar to Sine Saloum in Casamance [47] (Figure 1B).

Dakar represents the natural border between them, with distinct geomorphological and sedimentary characteristics [48]. The waves strongly impact the morphological evolution of this coast stretch, which controls the erosion and accretion processes [4,6,7], depending on the season. Belonging to the Sahelo-Sudanian tropical domain, the site is characterized by the alternation of two contrasting seasons: the dry season (from November to May) and a shorter wet season (from June to October) with the passage of the InterTropical Convergence Zone (ITCZ) in July [4]. The dry seasonal regime is characterized by the predominance of north, northeast, and east winds, while the humid seasonal regime is dominated by western, southern, and southwestern winds.

2.2. Waves Characteristics and Coastal Hydrodynamic

There are four types of wave regimes reaching the Senegalese Coast, depending on the season: (1) north–west swells generated by Westerly storms from the North Atlantic mid-latitude [49]. These long swells are the highest on the Big coast and present throughout the year but dominate the sea state during the dry season from November to June; (2) wind sea generated by both Northern and Southern Hemisphere trade winds year-round; (3) southwest swells from July to October, coming from the South Atlantic, and are almost always observed during the rainy season. These long-period swells mostly reach the Small coast with maximum power in August and September. More episodically, (4) West Atlantic swells are generated by tropical hurricanes that develop between the Cape Verde Archipelago and the Caribbean Sea from August to November [4,7,48]. The region is not directly affected by major storms or cyclones, but the signals of these distant, high-energy events can be seen in the wave climate [4,7]. Generated by oblique waves reaching the coastline, longshore transport plays a major role in the sediment dynamics of this coast [4,7]. The tide is semi-diurnal along the entire coast with a microtidal range (tidal range < 2 m).

3. Methodology

3.1. WaveWatch III Model Description

WaveWatch III[®] ([50–52], hereafter, WW3) is a third-generation wave model developed at NOAA/NCEP in the spirit of the WAM model [53–55]. WW3 is a widely used spectral model for wave hindcast and forecast in ocean engineering and Earth sciences. In WW3, the Wave Action Equation (WAE) is solved using a splitting method to treat in different steps spatial propagation, intra-spectral propagation, and source term integration [56–58]. A more comprehensive description can be found in The WaveWatch III[®] Development Group [58].

3.2. Forcing Fields: Wind Forcings, Bathymetry and Topography

The accuracy of modeled wave data directly depends on the quality of the forcing fields. The offshore morphology (topography/bathymetry, Figure 1A) data comes from GEBCO (2019) [59], while the coast benefits from specific bathymetric surveys. Wind forcing comes from the ERA5 reanalysis [60], with a 3-hourly time resolution and a spatial resolution of 0.5° for the Atlantic Ocean and 0.25° for the high-resolution grid nested on the Senegalese shelf. Several studies have confirmed the good quality of this wind forcing for wave prediction [61]. Although ERA5 provides very skillful surface winds (for non-extreme conditions), substantial negative biases can occur for wind speeds above 20 m/s [62–64]. To overcome this problem, Alday et al. [61] proposed a specific calibration of the source terms and a correction for wind speeds above 20 m/s.

3.3. Model Implementation

A 42-year wave hindcast from 1980 to 2021 was carried out over the whole Atlantic Ocean, with a high-resolution nested grid on the Senegalese Coast (local scale). To simulate the wave climate at these two scales, a one-way nesting strategy was adopted involving two computational grids: (1) a regional grid covering the North Atlantic Ocean, from 80° W to 20° E in longitude and from 70° S to 70° N in latitude, with a resolution of 0.5° × 0.5° (Figure 1A); (2) a local grid extending from 18° W to 16° W in longitude and from 12° N to 16.50° N in latitude, using a spatial resolution of 0.05° × 0.05° (Figure 1). The regional hindcast simulation was done first to generate spectral forcing along the boundary of the local grid. The spectral space was discretized using 24 evenly spaced directions over 360° and 36 logarithmically spaced frequencies ranging from 0.036 Hz to 1 Hz, with a 1.1 increment factor. Both grids were forced by the ERA5 winds. The wind input source term and dissipation by whitecapping used the ST4 (“test 475”) parameterization described in Alday et al. [61]. The Discrete Interaction Approximation (DIA, [65]) was used to represent the 4-wave nonlinear interactions. The wave-current interactions were not taken into account because mean currents on the shelf are relatively weak and the ~5 km

resolution does not allow for nearshore dynamics. The water level is considered constant in the simulations from the regional grid to the Littoral zone.

3.4. Wave Data Source

Wave field data come from MELAX, a coastal moored air-sea buoy deployed south of Dakar ($14^{\circ}20.8' \text{ N}$ – $17^{\circ}13.68' \text{ W}$, Figure 1). This multiparameter station includes a NORTEK AWAC at 35 m water depth (and about 25 km from the shore), which consists of a Doppler current profiler mounted with a pressure sensor and an acoustic tracking system (AST). The AST allows for a direct measure of the free surface elevation, overcoming the exponential attenuation of the pressure signal with depth. The despiking algorithm of Goring and Nikora [66] was applied to the AST signal in order to remove several spurious spikes. The AWAC data consists of hourly bursts of 20 min at 2 Hz (2400 points), including bottom pressure, AST data, and near-bottom velocities. However, orbital wave motions were too much damped by the 35 m water depth to compute directional wave spectra, and the analysis was therefore restricted to 1D frequency spectra. Power spectral density (PSD) estimates were computed using a fast Fourier transform with 10 Hanning-windowed segments (20 apparent degrees of freedom). These PSDs were integrated between a low-frequency cutoff F_{\min} set at half of the peak frequency and a high-frequency cutoff set at 0.3 Hz to compute wave bulk parameters such as the significant wave height H_s , the peak period T_p , and the mean wave period T_{m02} . One-dimensional spectra from the model were integrated over exactly the same frequency range as the data, thereby providing a consistent comparison.

3.5. Model Validation and the Wave Climate Analysis

Simulations provided time series of significant wave heights (H_s), mean wave directions (DIR), mean (T_{m02}), and peak (T_p) periods with an hourly interval. The local wave model outputs on the Senegalese Coast were then validated based on the MELAX data. Due to intermittency in the recorded data of the MELAX buoy, the model validation was only possible over the period from July 2019 to the end of March 2020. Bias and Root Mean Square Discrepancy (RMSD) were computed for all parameters, and RMSD was normalized by the mean of the observed values (NRMSD). Over the whole simulated period (42 years), boreal seasonal means were computed for winter (from 1 December to 1 March), spring (from 1 March to 1 June), summer (1 June to 1 September), and autumn (1 September to 1 December) in order to study the spatial and seasonal variability of the wave climate on the coast of Senegal. The particular choice of these boreal seasons in contrast to the local ones is supported by previous research showing that this coast is strongly influenced by the swells that develop at high latitudes, both north and south. In order to understand the causes of the observed variability, the SAM index was obtained from the British Antarctic Survey (BAS, www.nerc-bas.ac.uk/icd/gjma/sam.html, accessed on 1 February 2023) (Marshall et al. [34]). The North Atlantic Oscillation Index (station-based), proposed by Hurrell and made available through the NCAR National Center for Atmospheric Research (NCAR), can be accessed at (<https://climatedataguide.ucar.edu/climate-data/hurrell-north-atlantic-oscillation-nao-index-station-based>, accessed on 1 February 2023). Other Northern Hemispheric Teleconnection Indices were investigated (East Atlantic and Scandinavian modes) with data provided by Comas-Bru and Hernández [67], derived from instrumental data (<https://doi.org/10.1594/PANGAEA.892768>, accessed on 1 March 2023). These climate indices were selected because the associated climatic modes are known to explain the main part of the atmospheric variability in the Atlantic Ocean. Indeed, NAO, EA, and SCAN are the leading modes of climate variability for the North Atlantic Ocean, and they can be recovered from rotated principal component analysis of sea-level atmospheric pressure fields [40]. SAM is the leading mode of climate variability in the South Atlantic Ocean and corresponds to the leading empirical orthogonal function (EOF) in many atmospheric fields, including surface pressure, geopotential height, surface temperature, and zonal wind [34]. SAM is characterized by a large-scale alternation of atmospheric mass

between the mid- and high-latitudes associated with a meridional shift in the atmospheric westerly winds [15,34] at latitudes where the swells reaching Senegal are formed. Trends were estimated using robust regression approaches [20], the Sen slope method, and the linear regression method (although resulting in similar values in the end). Two statistical tests were used: (1) the Pearson correlation test to quantify possible links between wave parameters and the climatic modes; and (2) the Mann–Kendall significance test to determine the significance at the 95% confidence interval ($p \leq 0.05$) in the observed trends and correlations analysis.

4. Results

4.1. Model Predictive Skills

The wave parameters from the model outputs show overall good agreement with MELAX buoy observations, as shown in Figure 2. Indeed, the RMSD (NRMSD) for H_s , T_{m02} , and T_p are respectively 0.12 m (13.64%), 0.90 s (12.46%), and 2.25 s (19.99%). While no bias is observed for H_s , slight positive biases of 0.24 s and 0.53 s are observed for T_{m02} and T_p , respectively. At the location of the MELAX buoy (25 km off the coast, 35 m water depth), this new hindcast brings major improvements in terms of wave bulk parameters compared to ERA5, with errors decreasing by 3 for H_s and by 50% for T_{m02} . Only T_p is slightly better represented in ERA5. This comparison also suggests that direct outputs of ERA5 can only be used in deep waters and not to investigate wave climates along the coastline of Senegal. Although the observations are not continuous over the validation interval, the model shows a fairly good ability to hindcast the extreme H_s and T_{m02} values (min, max). All wave parameters, H_s , T_p , and T_{m02} , provided from this model, give NRMSD (in between 12.46–19.99%) corresponding to the state of the art (e.g., [61,68]). Once integrated over one month, these errors drop to 2–3%, which suggests that our hindcast is accurate enough to investigate wave climate based on seasonal means.

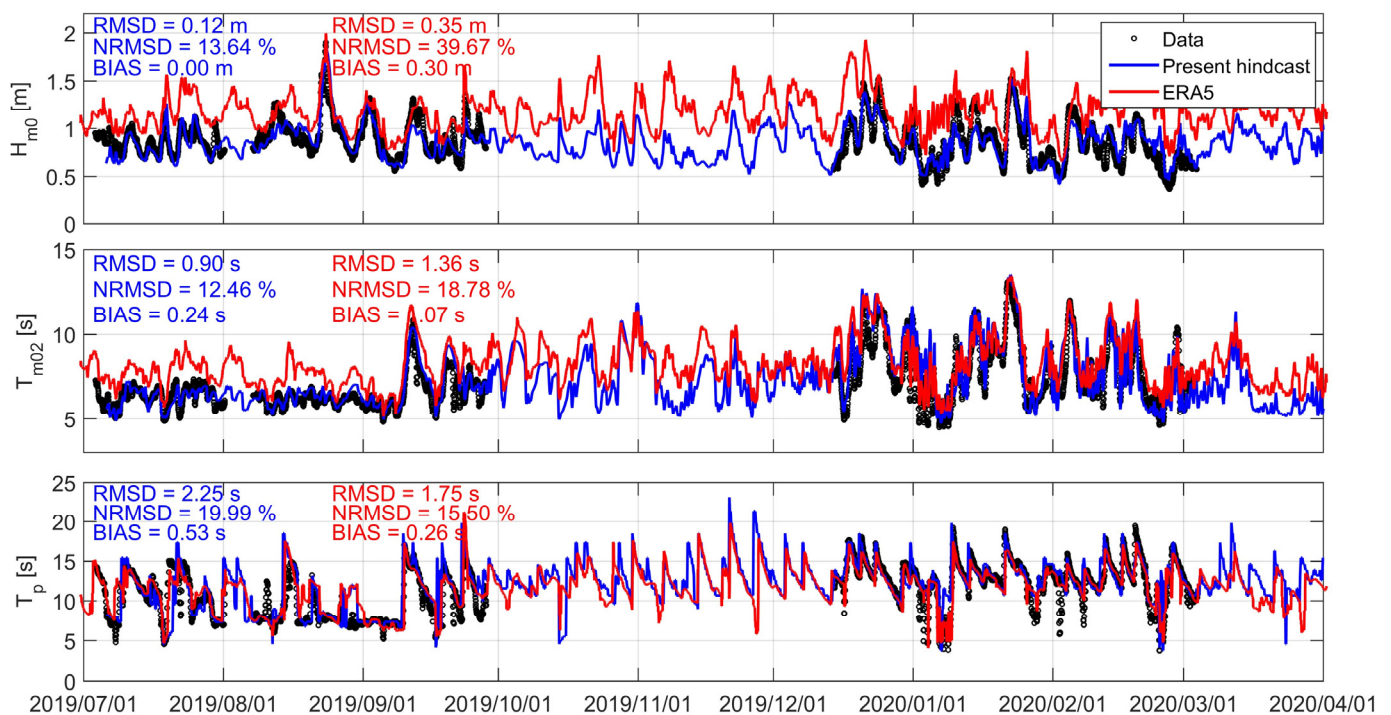


Figure 2. Comparison between wave bulk parameters (significant wave height (H_s , top panel), mean wave periods (T_{m02} , middle), and peak periods (T_p , bottom panel)) computed from the MELAX buoy (black) and model results from the new hindcast (blue) and retrieved from ERA5 (red) from July 2019 to March 2020 at the location of the MELAX buoy (located by 35 m water depth, Figure 1B).

4.2. Description of Wave Climate

4.2.1. Mean and Extreme Conditions

The mean distribution of wave parameters over the studied period shows significant spatial variability (Figure 3), off the coast in general and along the Small coast in particular. On average, H_s are about twice as high on the Big coast (1 to 1.2 m, from Saint-Louis to Dakar) than on the Small coast (0.4 to 0.6 m, from Dakar to the Southern Coast extremity). On average, the Dakar Peninsula is the part of the Senegalese Coast most exposed to waves, with H_s ranging from 1.2 to 1.4 m. H_s are strongly attenuated to the south given their spatial distribution on the shelf of the Small coast. In front of the Big coast, wave directions range from 320° to 330° , highlighting their Northwest Atlantic origin. This is similar off the Small coast (270° – 310°), but a peculiarity is clearly observed south of Dakar. Swells refract around the Dakar Peninsula so that their direction rotates from NW (320°) to the north to SW (220°) to the south. The peak swell periods are shorter off the Big coast (~ 10 s) than the Small coast (~ 11.5 s).

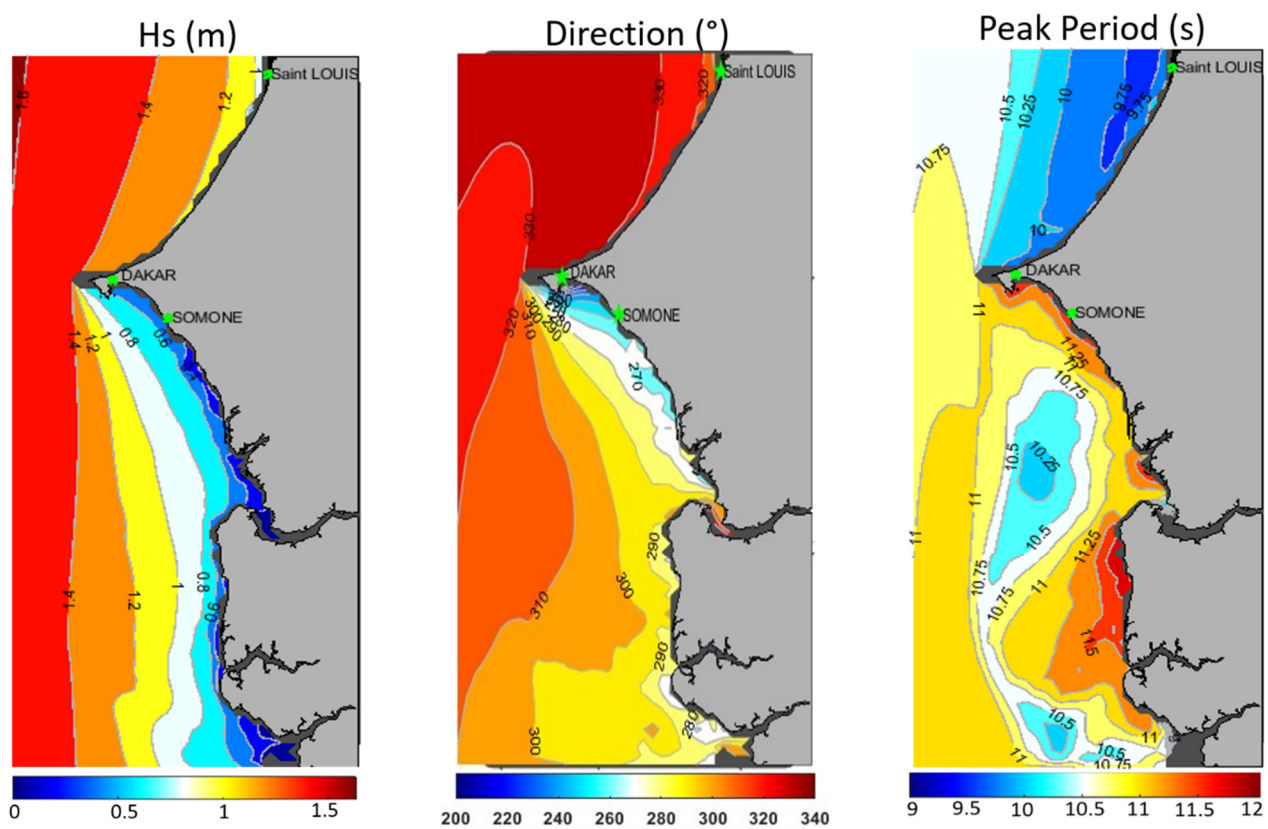


Figure 3. Spatial maps of the yearly mean wave climate, significant wave height (H_s (m), **left**), mean wave direction (DIR ($^\circ$), **middle**), and peak period (T_p (s), **right**) computed on the Senegalese Coast from 1980 to 2021 (Brown patches along the coastline denote areas with insufficient resolution).

The spatial analysis of the extreme wave climate on the coast was carried out based on the 90th, 99th, and 100th percentiles of H_s values and peak T_p periods (Figure 4). The spatial distribution of the 90th percentiles of H_s shows similarities with the mean H_s , although with values about 40% larger. The 99th and 100th percentiles also show similar patterns but with values, respectively, two and three times larger than the mean H_s . According to the spatial distribution of each H_s percentile observed over the study period, the extreme swells that whip the coast of Senegal are always higher by at least 1 m on the Big coast than the Small coast. Dakar is the vanguard part of the coast, most exposed to maximum heights (up to 3 m to 3.5 m). The peak period T_p varies from ~ 13 s to 14 s at the 90th percentile to ~ 14 s to 16 s at the 99th percentile and from 18 s to 22 s for the maximum peak periods. This suggests a fairly distant origin of the swells during extreme events.

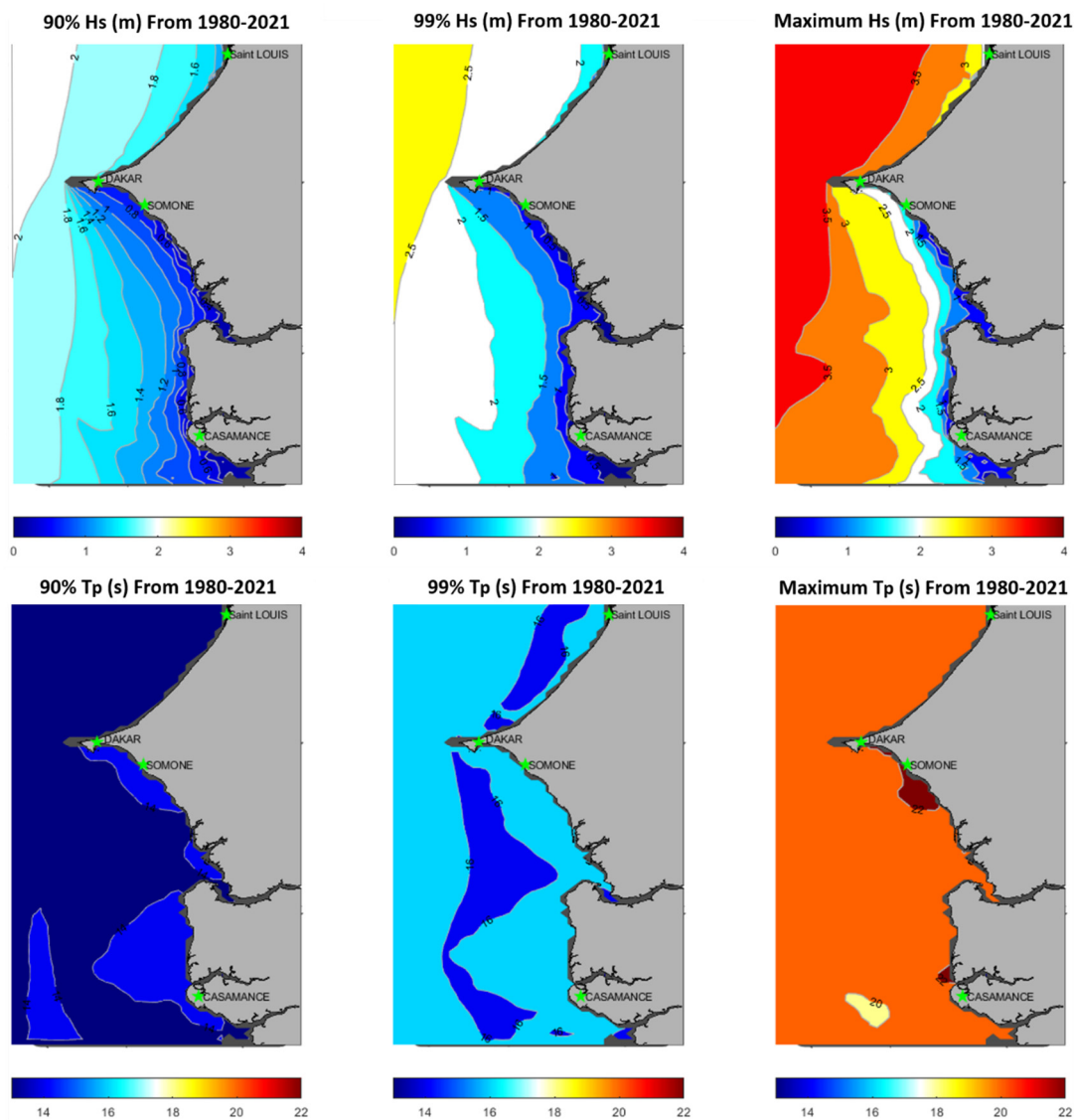


Figure 4. Spatial maps of extreme wave climate conditions for significant wave height (H_s (m), **top**) and peak periods (T_p (s), **bottom**), respectively, at the 90th, 99th, and 100th percentiles of maximum values on the Senegalese Coast from 1980 to 2021 (Brown patches along the coastline denote areas with insufficient resolution).

4.2.2. Seasonal Variability

At the seasonal scale, waves on the Senegalese Coast present strong spatial variability for the studied parameters (Figure 5). For H_s , the highest values (~ 1.6 m) are found during the boreal winter and spring, with smaller values in autumn (~ 1.4 m) and summer (~ 1.2 m, about 40% less). The winter and spring present the strongest wave conditions on the Big coast (from 1.2 to ~ 1.4 m and ~ 1.6 m off Dakar). On the contrary, the summer represents the season endowed with higher waves reaching the Small coast, with $H_s \sim 0.6$ m, which is about 50% more than other periods (with ~ 0.4 m on average). Dakar constitutes a natural border, for which the waves reaching the coast in all seasons are at least double in the north on the Big coast compared to the Small coast in the south. Overall, the average directions of the waves are west to north–west (270° – 330°) in winter, spring, and autumn, while in summer, the south of the Small coast has rather west to south–west directions (240° – 270° and $>240^\circ$ between Dakar and Somone). The directions on the Big coast remain north–west (300° – 330°), suggesting that Southwestern swells do not reach this stretch of coast. For peak periods, winter exhibits the highest T_p with, on average, fairly uniform T_p conditions

along the entire coast (~12 s). The peak period conditions are spatially roughly similar between spring and autumn and vary between 10–11.5 s. Summer conditions overall show the lowest T_p (from 8–9.5 s to the north, from 9–11 s to the south) compared to other seasons.

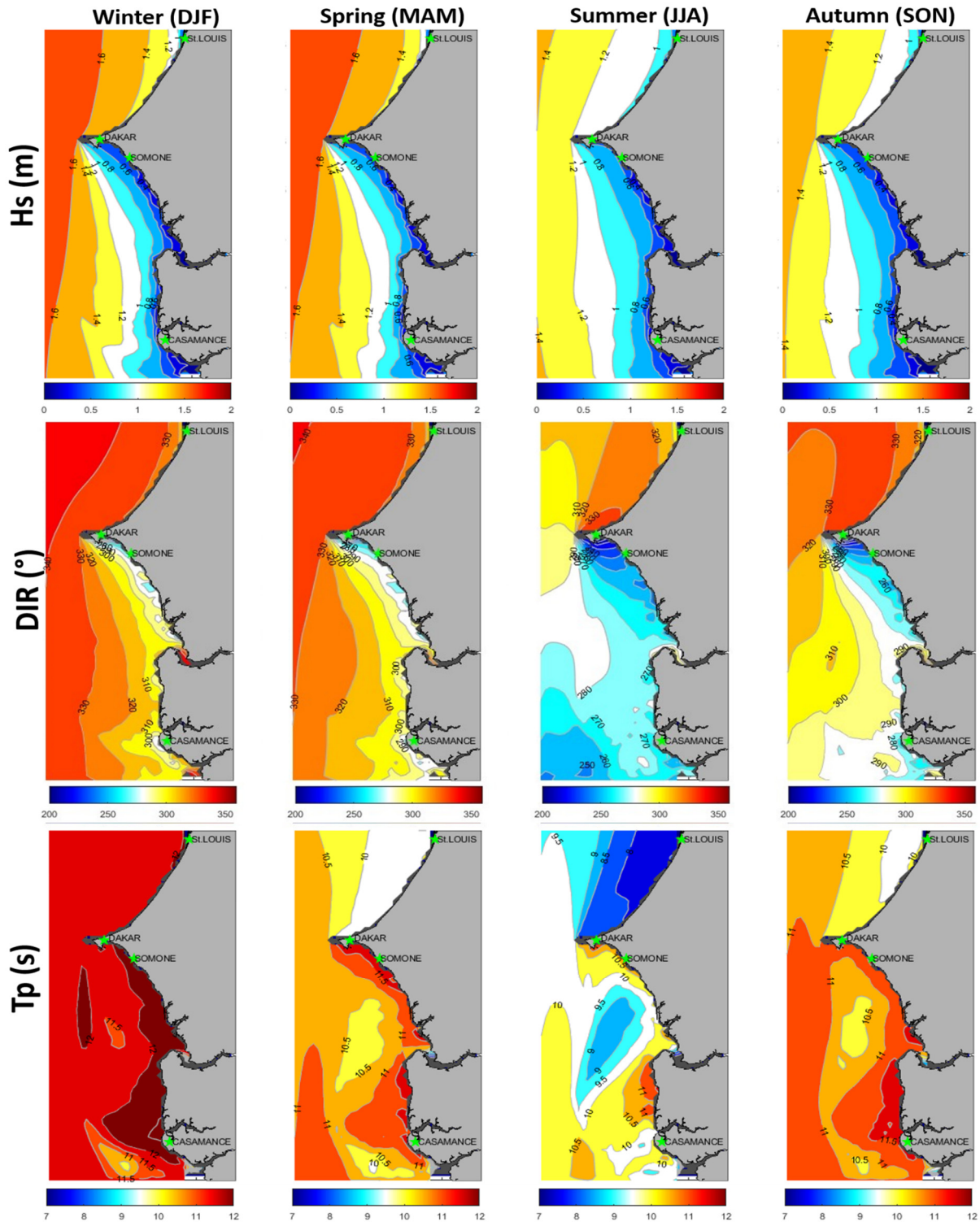


Figure 5. Spatial maps of seasonal mean wave climate: significant wave height (H_s (m), **top** panel), mean wave direction (DIR (°), **middle** panel), and peak period (T_p (s), **bottom** panel) computed on the Senegalese Coast from 1980 to 2021. The dark grey patches along the coastline denote areas of insufficient model resolution.

4.2.3. Long-Term Trends

The global trend analysis of wave parameters over the studied period (1980–2021) shows very high spatial variability, as presented in Figure 6. The non-hatched areas correspond to the areas where trends are significant, with a 95% confidence level based on a Mann–Kendall test. Wave H_s globally show significant positive trends on the Senegalese Coast, with values increasing from nil to weak values off the Big coast (0–0.06 cm/year, from St-Louis to Dakar) to the Small coast (>0.06 cm/year), where maximum values up to 1.2 cm/year can be seen offshore of Casamance. For the wave periods (T_{m02} , T_p), the trends observed are extremely weak overall (the maximum is about 5.10^{-3} s, ~ 0.5 s per century). The mean period T_{m02} shows positive trends over the entire Littoral (between 0.001–0.0045 s/year), but they are maximum (0.0025–0.0045 s/year) and significant (with 95% confidence) only off the Dakar Peninsula and its surroundings. The peak periods T_p have positive trends (0–0.006 s/year) along the coast but maximum and significant only off Saint-Louis (0.004–0.006 s/year). Wave mean directions show a counterclockwise rotation over the study area, ranging from -0.12° to -0.02° /year.

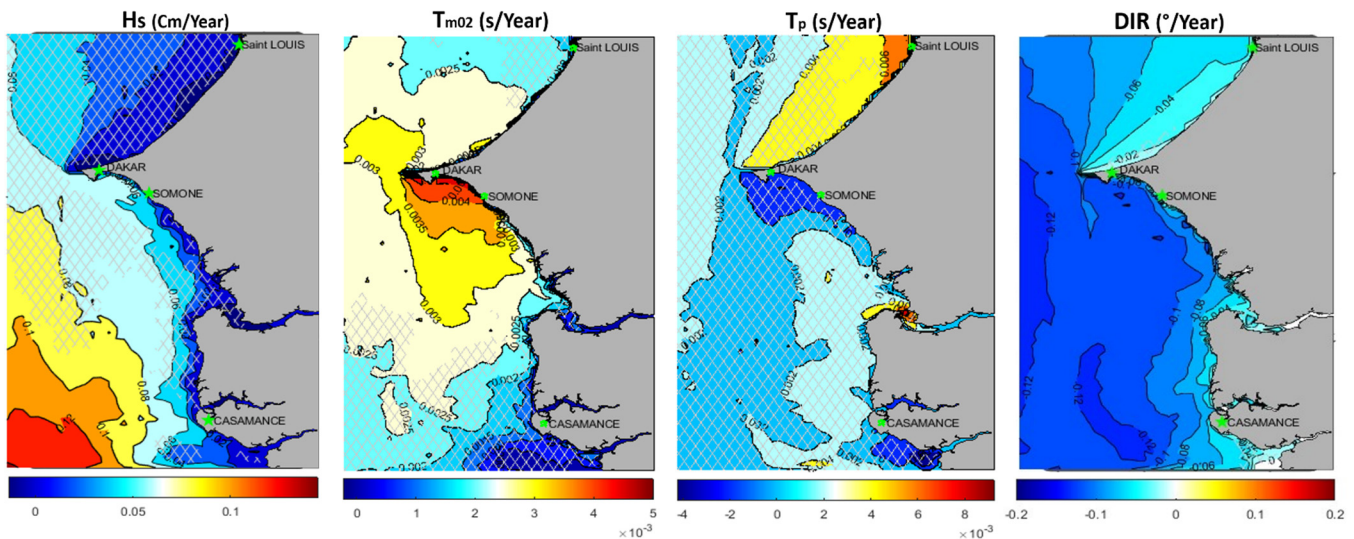


Figure 6. Trends of wave parameters (from left to right), significant wave height (H_s (cm)), wave mean period (T_{m02} (s)), peak period (T_p (s)), and mean direction (DIR ($^\circ$)) computed on the Senegalese Coast from 1980 to 2021, Hatched zones on maps indicate areas where trends are not significant at 95% (Mann–Kendall test).

The analysis of the interannual seasonal trends obtained from the different wave parameters shows an important spatial variation (between the Big and Small coasts) within a singular boreal season and over all seasons compared to each other (Figure 7). Regarding H_s , maximum and significant trends are found during the summer off the Small coast (0.2 cm/year), which decreases towards the north up to the Dakar Peninsula (0.1 cm/year). The trends observed in the mean wave directions show an anticlockwise rotation that is almost negative (between -0.25 and 0° /year) and significant only during summer and autumn (95% confidence). The observed DIR during these seasons show similarities marked by a decrease from the open sea (-0.03° /year) towards the shore (-0.05° /year) and a spatial difference of $\sim 0.05^\circ$ /year between autumn and summer. Positive and significant T_{m02} trends (95% confidence) are observed during summer and autumn, with maximum values in the northern part of the Small coast (~ 0.004 s/year and ~ 0.007 s/year, respectively). Overall, the observed T_p trends are found to be significant (95% confidence) only during autumn near the Big coast shore with ~ 0.015 s/year, about 20 times higher than the observed T_{m02} maximum trend.

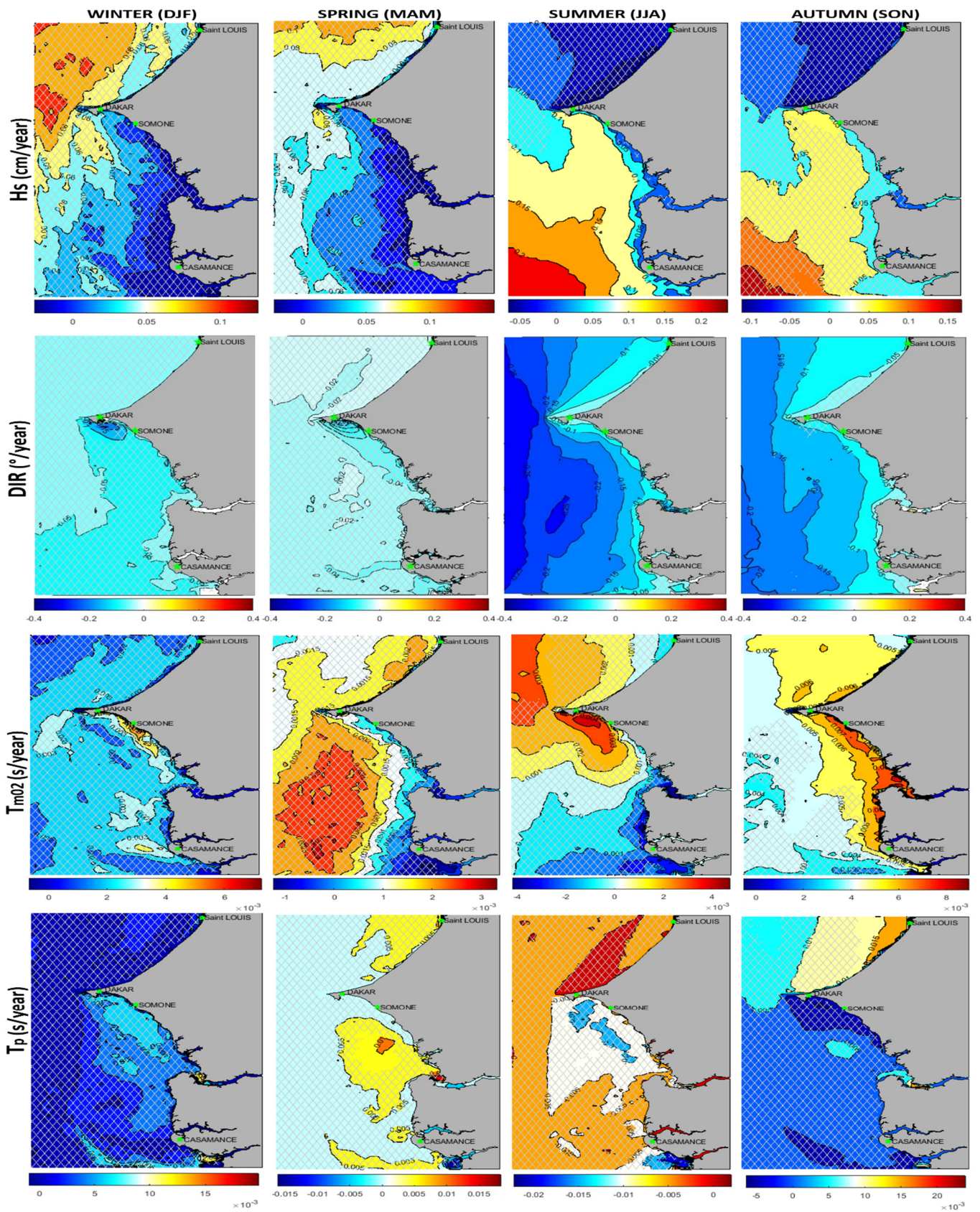


Figure 7. Seasonal trends computed over the period 1980–2021 for the main wave parameters (Hs, DIR, T_{m02}, and T_p) in winter, spring, summer, and autumn on the Senegalese Coast from 1980–2021, Hatched zones on maps indicate areas where trends are not significant at 95% (Mann–Kendall test).

5. The Control of Atlantic Climate Modes on Wave Climate Variability on the Senegalese Coast

In order to understand the origin of the patterns and trends described in the previous section, a correlation analysis was performed between fields of mean wave parameters (H_s , T_{m02} , T_p , and DIR) and the indexes of the main mode of climate variability for the North (NAO, EA) and the South (SAM) Atlantic Oceans.

5.1. The North Atlantic Oscillation (NAO)

The correlation between the NAO index and the mean wave parameters (H_s , T_{m02} , T_p , and DIR) was computed over the studied area from 1980 to 2021. The results are only presented for the boreal winter (DJFM), as it is the only season where both the strongest and most significant correlations were found (Figure 8). Strong negative and significant correlations (95% confidence) are generally observed for H_s and T_{m02} , while DIR spatially presents a positive and significant correlation, particularly off the Big coast. H_s and NAO are strongly negatively correlated with values of -0.6 on the 'Big coast' and up to -0.7 on the 'Small coast' (e.g., Dakar and Somone vicinities). Similarly, the wave mean period T_{m02} and NAO present a negative correlation of -0.5 on almost the entire coast, only decreasing until being non-significant in Casamance. Weaker and non-significant negative correlations are observed between T_p and the NAO, between -0.2 and -0.3 . The correlations between DIR and NAO are exclusively positive, significant off the north of the Small coast with 0.4 and along the whole Big coast, where correlations are stronger with 0.5 . These positive correlations mean that positive phases of NAO are associated with waves coming from further north and vice versa.

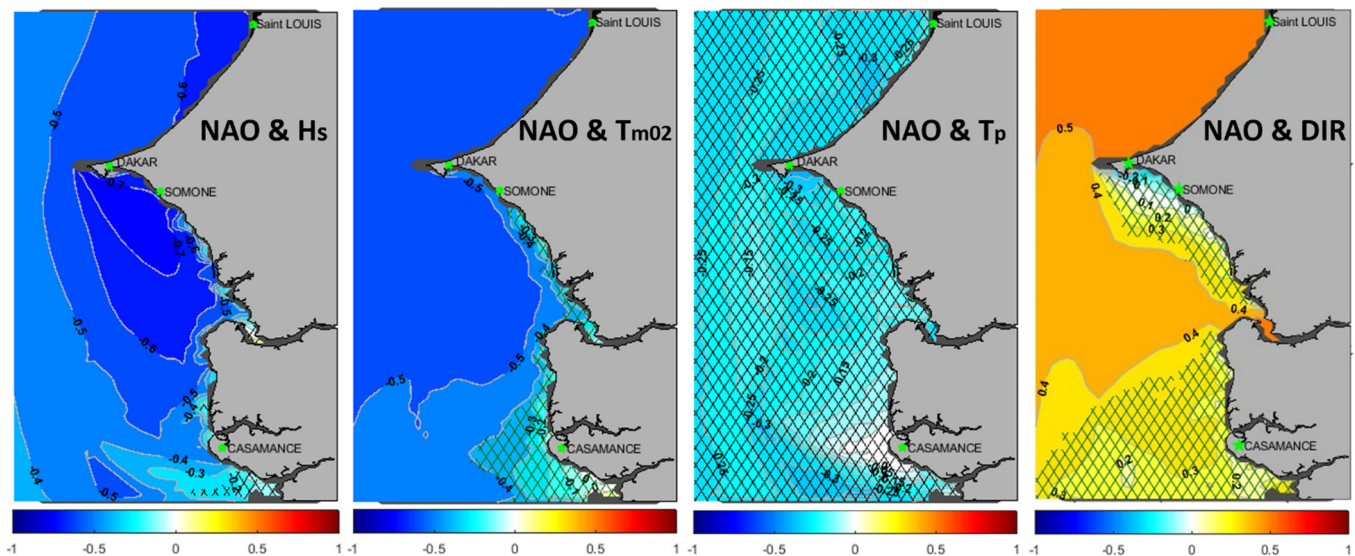


Figure 8. Spatial correlations between NAO and wave parameters (H_s , T_{m02} , T_p , and DIR) during boreal winter (DJFM), computed on the Senegalese Coast from 1980–2021, crosslines on maps indicate areas with non-significant correlations (at 95% confidence interval from Mann–Kendall test).

Seasonal wind fields were computed from ERA5 to explain the correlations found between wave parameters and the main climatic modes (Figure 9). These wind fields correspond each time to the norms of the zonal and meridional components. To ease this analysis, the period characterized by the largest values of the corresponding indices were considered: winter 1989 (December 1988 and from January to March 1989) for the NAO+ phase (+2.86) and winter 2010 (December 2009 and from January to March 2010) for the NAO− phase (−2.7085). The spatial repartition of wind fields shows opposing patterns during NAO+ and NAO− phases in the North Atlantic Ocean (Figure 9). Thus, during NAO positive phases, westerlies are stronger but shift northward by 1000 to 2000 km compared to negative phases. The NAO− phases are characterized by less intense depressions

but are shifted to the south around latitudes 30° N to $\sim 20^{\circ}$ N. Under negative phases, fetches are located closer to Senegal, which directly explains the negative correlation between Hs and NAO indices. Fetches that shifted northward during positive phases also explain the positive correlation between these indices and the mean wave direction, DIR. Previous studies already reported larger waves in Southern Europe under negative phases of NAO (e.g., [12,14,31–33,40]). In this study, we show that this control is also active until the coastlines of Senegal and impacts all studied wave parameters.

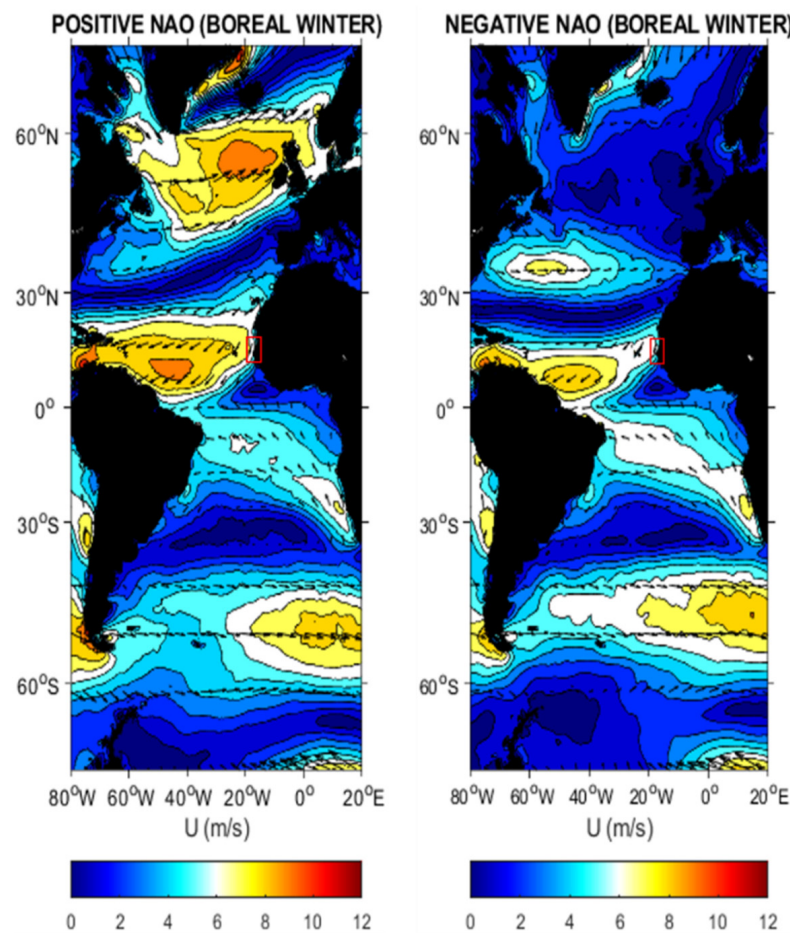


Figure 9. The red rectangle indicates the average winter wind speed corresponding, respectively, to the periods of maximum (NAO+, left) and minimum (NAO-, right) phases of NAO in the tropical Atlantic on the Senegalese Coast.

5.2. East Atlantic Mode (EA)

The same analysis was performed for the East Atlantic index (hereafter, EA) for the boreal winter (DJF, Figure 10) from 1980–2016 (see Section 3.5). Strongly negative significant correlations are obtained in boreal winter for Hs (-0.6 to -0.8), T_{m02} (-0.5 to -0.7), and T_p (-0.75 to -0.8). For DIR, similar patterns are obtained for the EA as for the NAO, with positive correlations off the Small (0.4 to 0.5) and all over the big coast (0.3 to 0.4) from Dakar to Dakar to Saint-Louis. Similarly to NAO, but with stronger and more significant values, a positive correlation area develops to the west of Casamance. The remote/teleconnection of the wave parameters to the EA mode remains observed on the Senegalese Coast during the boreal spring (not shown). However, the signal is weakened given the moderately negative and significant correlations observed offshore between Hs and EA (-0.4 to -0.5), T_{m02} and EA (-0.3 to -0.4), and T_p and EA (-0.4 to -0.5).

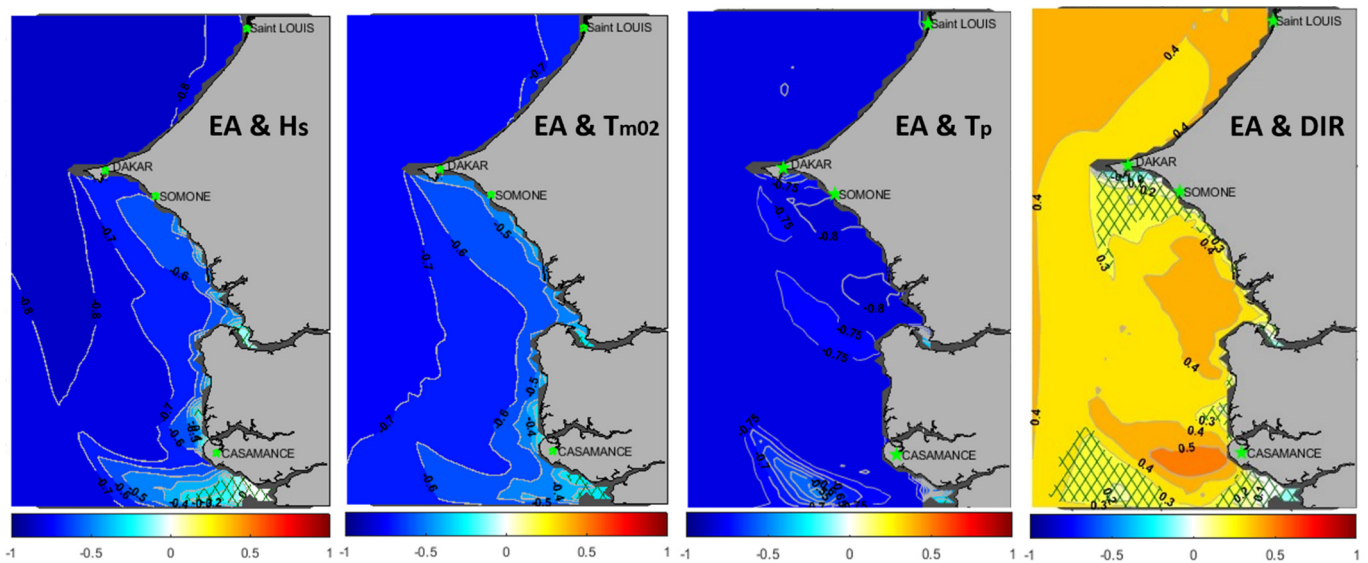


Figure 10. Spatial correlations between East Atlantic mode (EA) and wave parameters (H_s , T_{m02} , T_p , DIR), computed on the Senegalese Coast from 1980–2016 in boreal winter (DJF), crosslines on maps indicate areas with non-significant correlations (at 95% confidence interval, Mann–Kendall test).

Spatial wind patterns associated with positive and negative phases of EA were also compared (Figure 11). These wind fields correspond to the norms of the zonal and meridional components. The extreme index used corresponds to +EA (+1.51) during winter 2005 (December 2004 and from January to February 2005), while $-EA$ (-1.71) occurs in winter 2014 (December 2013 and from January to February 2014). The spatial patterns of wind fields, respectively, for the positive and negative phases of EA (Figure 11) show many similarities with those observed in NAO (Figure 9). Compared to EA+ phases, EA– phases are characterized by fewer hollow depressions but are shifted to the south around latitudes 35° N to $\sim 25^\circ$ N. During EA positive phases, westerlies are less strong but also shift more northward by 1000 km compared to EA negative phases. Although more northward, westerlies are much stronger during EA– phases (with $\sim 3 \text{ m}\cdot\text{s}^{-1}$ greater than during NAO– phases). Fetches are thus located a little further from Senegal but endowed with stronger winds. This explains the strong negative correlation observed between wave parameters and EA indices. A few previous studies have already reported larger waves in Europe and North Africa under negative phases of EA (e.g., [31,32,38,40]). This study reveals that EA control is active at lower latitudes in the North Atlantic, like Senegal. Some studies have also found a link between the Scandinavian mode (SCAN, the third mode of variability in the North Atlantic) and wave climate variability (e.g., [33,38–40]) at similar latitudes. Still, no correlation has been found between the SCAN mode and the wave variability in this study area. Similarly, no links were found between the Pacific Ocean’s leading mode of variability, ENSO, even considering its negative $-ENSO$ (El Niño) and positive $+ENSO$ (La Niña) phases independently.

5.3. South Atlantic Oscillation (SAM)

The correlation analysis between the SAM index and the wave parameters (H_s , T_{m02} , T_p , and DIR) showed almost no significant relations (correlation between -0.1 , 0 , and 0.1 , not shown here). On the other hand, while only considering positive phases (SAM index > 0 , hereafter, +SAM), significant correlations with H_s are found during boreal summer (Figure 12). Correlations with the other wave parameters (T_{m02} , T_p , and DIR) were very weak and all non-significant. During summer (JJA), H_s and +SAM only show significant local correlations off the Small coast, reaching 0.45 . Reguero et al. [69] found similar spatial correlations for the monthly mean H_s and SAM in the central West Pacific (at similar latitudes).

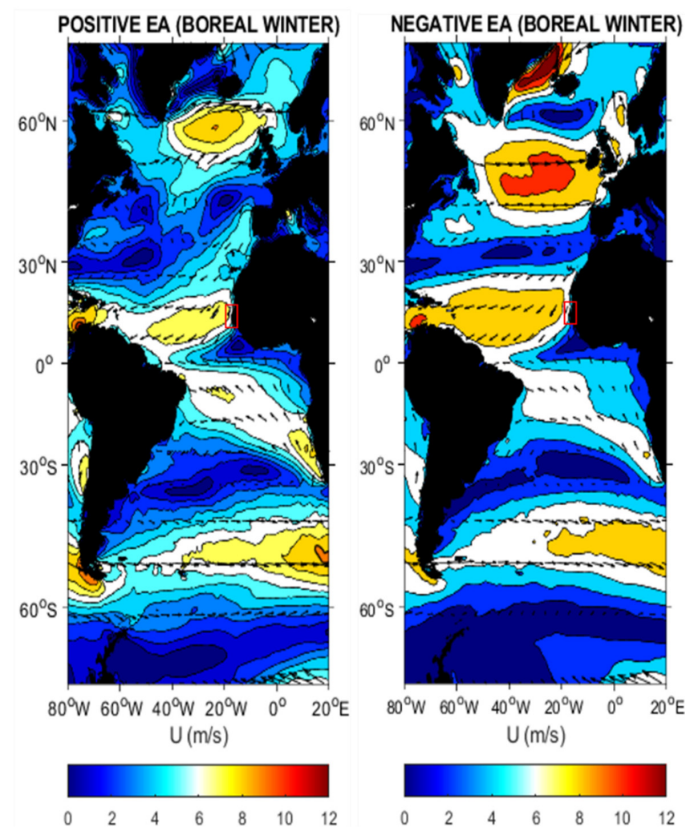


Figure 11. The red rectangle indicates the average winter wind speed corresponding, respectively, to the periods of maximum (EA+, left) and minimum (EA−, right) phases of EA mode in the tropical Atlantic on the Senegalese Coast.

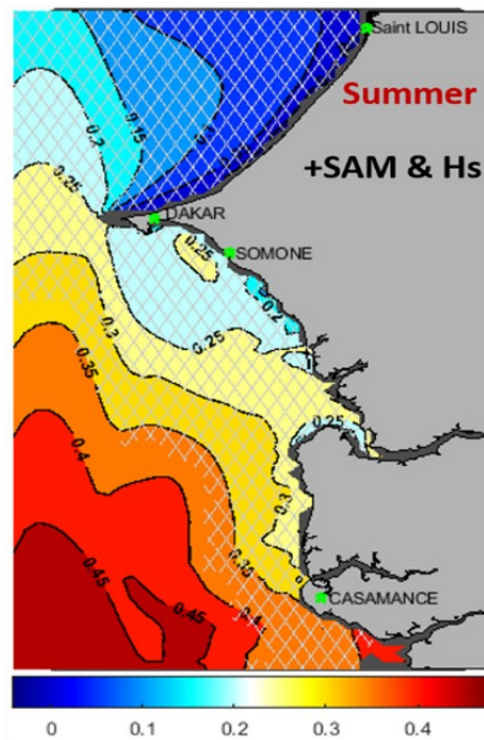


Figure 12. Spatial correlations between the +SAM index and Hs during boreal summer, computed on the Senegalese Coast from 1980–2021, indicated that crosslines on maps indicated not significant areas (at 95% confidence interval, Mann–Kendall test).

Seasonal wind fields were also computed from ERA5 to explain the correlations found between H_s and +SAM. During boreal summer (Figure 13), the extreme positive and negative SAM indexes used correspond, respectively, to 4.060 (summer 2010; JJA) and -3.160 (summer 1995; JJA). The +SAM phases in boreal summer are characterized by stronger westerlies at latitudes 40°S – 65°S in the storm belt over the Southern Ocean [15], where the southwest swells reaching Senegal (the Small coast from July to October) develop. This explains the more energetic wave conditions associated with +SAM observed on the Small coast. In this region, previous works revealed that wave variability was linked exclusively to +SAM in the GG [45] in Senegal [7]. Marshall et al. [15] also reported that H_s correlated with the SAM in its high polarity (+SAM) during summer. They found strong positive wind anomalies (4–6 m/s) between latitudes 40°S – 60°S during +SAM phases in summer.

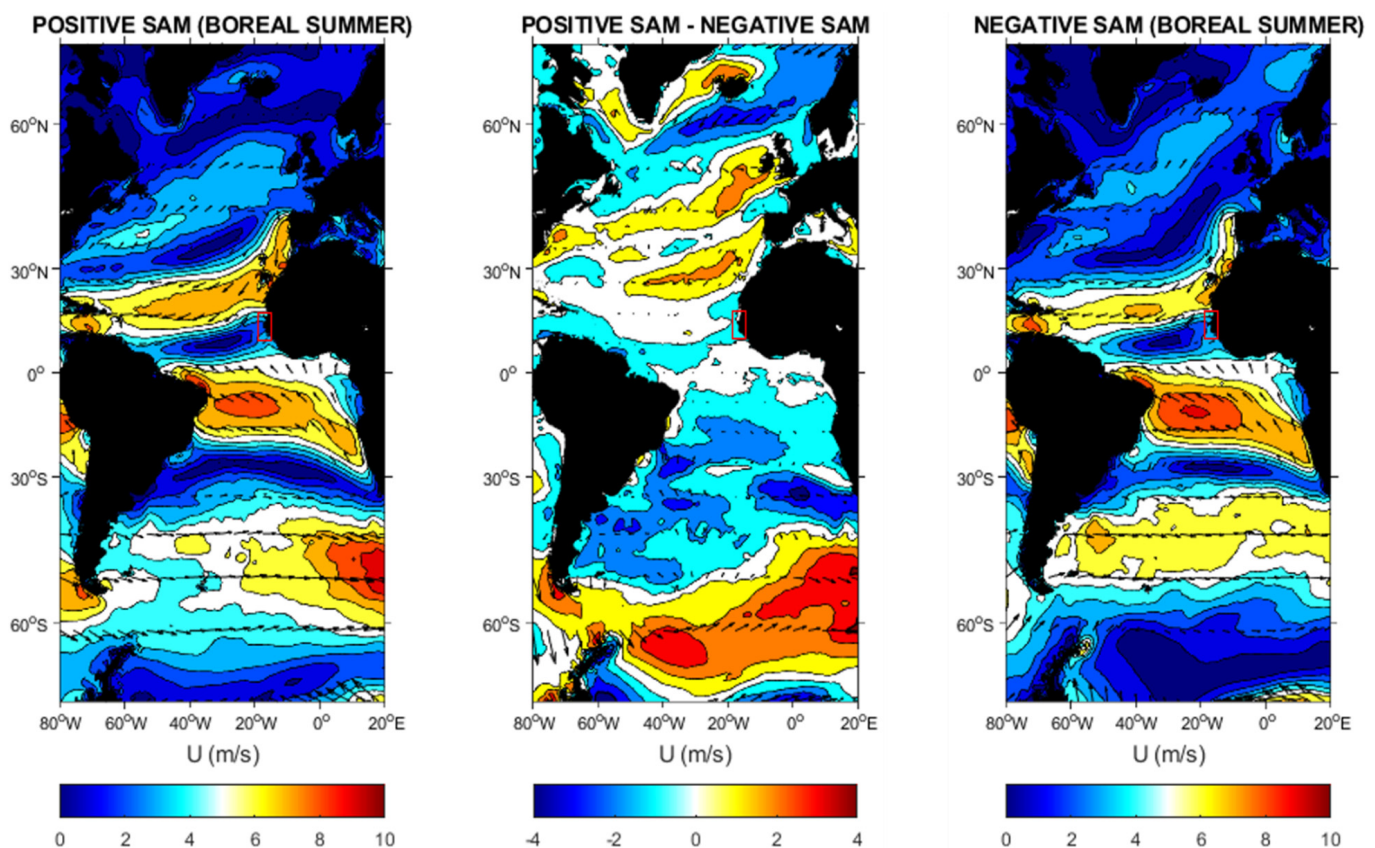


Figure 13. Average wind speed in the tropical Atlantic corresponds, respectively, to periods of maximum (+SAM, left) and minimum (−SAM, right) phases of SAM during boreal summer. The wind spatial difference is shown on the middle panel, and the Senegalese Coast is indicated by the red rectangle.

6. Discussion and Conclusions

6.1. Limitations of the Present Model

The wave climatology of the Senegalese Coast was analyzed based on a new wave hindcast from 1980 to 2021. This relies on the WW3 model implemented with high spatial (0.05°) and temporal (1 h) resolutions and state-of-the-art parameterizations for wind input and dissipation by whitecapping. Model/data comparison showed that the present configuration was able to reproduce well-defined wave parameters (H_s , T_{m02} , and T_p) with an accuracy comparable to previously published studies using high-resolution spectral wave modeling (e.g., [18,61,68]). The present hindcasts showed a substantial improvement compared to available wave hindcasts such as ERA5, which suggests that global hindcasts are too coarse to investigate wave climates along the coasts of Senegal. However, some

limitations remain. First, the model could not be verified on the Big coast because no observations were available. It is now possible to use the latest advanced altimetry data to obtain consistent wave observation up to ~10 km from the coast, compared to >100 km previously, but this was beyond the scope of this study. Other studies have shown that accounting for the nature of bottom substrates in wave dissipation by bottom friction can yield improved predictions compared to a spatially uniform representation, particularly in shallow depth (e.g., [68,70]). Although sensitivity analyses did not reveal a substantial effect at the location of the MELAX buoy, a more realistic representation of the substrate nature in the model could probably improve wave predictions nearshore, particularly over rocky bottoms (e.g., [70]).

6.2. Dakar Peculiarity in the Coastal Morphology

The spatial distribution for all the wave parameters showed a significant contrast between the Big and Small coasts on the mean, seasonal, and even in extreme wave climate conditions. These contrasting spatial patterns are largely controlled by the singular morphology of the Dakar Peninsula, which plays a key role in wave propagation on the Senegalese Coast by providing a natural barrier for swells originating from the north–west and the south–west. Throughout their propagation around Dakar Peninsula, NW swells rotate by about 50° to 100°. Their significant height is reduced by about 50% when reaching the Small coast, especially during seasons where the north swells are predominant. Locally, previous studies had already proposed that the decrease in H_s around Dakar is due to diffraction ([48,71]). However, this process is not dominant because diffraction is not accounted for in the model, while it should, on the contrary, add more energy to the Small coast (i.e., enlargement of wave fronts behind an obstacle). Hence, the dominant processes explaining spatial wave patterns around the Dakar Peninsula are refraction ([7,11]) combined with a strong shadow effect.

6.3. The Wave Climate Control by Atlantic Modes of Variability

Wave climate variability was linked to several Atlantic climate modes. Almar et al. [7] found a significant and negative correlation between NAO and H_s in boreal winters from 1980–2016. In the present study, we extended this correlation to other parameters, such as T_{m02} , which was negatively correlated with NAO, and DIR, which was positively correlated with NAO. The spatial patterns of correlations between T_{m02} and NAO were found to be similar to those observed between H_s and NAO. Interestingly, the East Atlantic mode (2nd Northern Hemisphere mode of variability) also showed robust links that explain the wave variability with strong negative correlations larger than those obtained with NAO during winter (and although weakened, significant negative correlations remain observable during spring). Links between SAM mode and wave variability are generally restricted to +SAM and H_s . The +SAM involved strong H_s conditions during the summer. Knowledge of these remote connections is interesting as it would indicate that lower-than-average wave energy conditions on the coastline would occur when the two modes, NAO and EA, are concomitantly endowed with their highest positive phase index. Similar observations characterized by several climatic modes active simultaneously have already been reported in the Atlantic (e.g., [16,32,33]). When it is possible to predict these modes on a seasonal scale or even further on a climate change scale, then an idea will be made of the future wave regimes on the Senegalese Coast (and in the region).

6.4. Long-Term Trends on Wave Parameters and Climate Modes, Comparative Evolution and Future Implications

While focusing only on significant trends at 95%, wave parameters show modest trends, although strong contrasts can be observed depending on the season. The climatology obtained on the coast shows very weak trends for the wave periods (T_{m02} and T_p , ~0.05 s per decade at maximum). The directions showed a counterclockwise relationship overall (between 0° and –1° per decade). These results on wave T_{m02}/T_p and DIR trends

corroborate well the findings of previous studies in GG ([17,18]). The results obtained from the Hs annual trends corroborate well the previous findings of Reguero et al. [69] from 1948 to 2008 for coasts of similar latitudes but to the west of the Atlantic Ocean. More locally, our upward trends in Hs reaching $\sim 1.2 \text{ cm.decade}^{-1}$ are in line with Osinowo et al. [18] from 1980 to 2016 and Dahunsi et al. [17] from 1979 to 2005 at the east of the GG, although both investigated the extreme wave climate (99th percentile). For a consistent comparison, a global trend computation on extreme Hs (99th percentiles, 1980–2021) over the study period also showed similar spatial patterns equivalent to the maximum trends observed by Osinowo et al. [18] in the Western part of the GG. Spatially highly variable, the trends obtained on mean Hs were shown to range from $0.2 \text{ cm.decade}^{-1}$ (Big coast) and $1.2 \text{ cm.decade}^{-1}$ (Small coast), with a maximum increase during summer (max $\sim 2 \text{ cm.decade}^{-1}$ over Small coast), which decreases from south to north. Overall, the observed Hs spatial patterns and trends would be mainly explained based on the activities of South Atlantic swells and storms. Over the study period, no trend can be observed for NAO and EA modes, with their corresponding indices dropping by $-0.003 \text{ .year}^{-1}$ and $-0.005 \text{ .year}^{-1}$, respectively. On the other hand, the SAM index shows an upward trend of $+0.07 \text{ .year}^{-1}$. For the other wave parameters, an increase in T_{m02} to the north of the Small coast and a counterclockwise rotation of DIR are observed in summer along the Small coast, i.e., when the wave climate is dominated by swells generated in the Southern Atlantic Ocean. As the wave climate in the Southern Atlantic Ocean is partly controlled by SAM [15,34], these trends are mostly explained by the increase in the SAM index by $+0.07 \text{ .year}^{-1}$ over the studied period. The Hs increase observed in this study is partly explained by the upsurge of South Atlantic storminess associated with SAM. Several recent studies have also relayed an increase in South Atlantic storminess (e.g., [15,16,72]), and other research has associated this upsurge with the strong positive trend observed on the SAM index (e.g., [7,15,34,42]). Similarly, Bertin et al. [14] found an increase in Hs in the North Atlantic Ocean over 1900–2008, a period during which the NAO index showed a very weak trend. These authors associate this increase with increased wind speeds supported by observations, although they did not provide a physical explanation. Young et al. [19] also reported such an increase in wind speed from 1985 to 2008 on a global scale. However, other aspects remain to be investigated, such as the distinctive climatology of wind waves and distant swells using partitioning algorithms [73,74] and the direct investigation of wind fields. Finally, the proposed wave model and results obtained from this study could guide future coastal research associated with this area, such as the morphodynamic evolution of beaches, estuaries, and coastal lagoons in large numbers on the Senegal Coast.

Author Contributions: Conceptualization, M.S.S., X.B. and I.S.; methodology, M.S.S., X.B. and I.S.; software, X.B. and M.S.S.; validation, X.B., M.S.S. and A.L.; formal Analysis, M.S.S. and X.B., investigation, M.S.S., X.B. and M.S.; resources, I.S., X.B. and M.B.D.; data curation, M.S.S., X.B., I.S., M.S. and A.L.; writing—original draft preparation, M.S.S.; writing—review and editing, M.S.S., X.B., I.S., A.L., M.S. and M.B.D.; visualization, X.B., I.S., M.B.D. and A.L.; supervision, X.B., I.S. and M.B.D.; project administration, X.B., I.S. and M.B.D.; funding acquisition, I.S., X.B. and M.B.D. All authors have read and agreed to the published version of the manuscript.

Funding: This research received no external funding.

Institutional Review Board Statement: Not applicable.

Informed Consent Statement: Not applicable.

Data Availability Statement: The wave hindcast presented in this study can be accessed through the Zenodo Repository number doi.org/10.5281/zenodo.8139334.

Acknowledgments: This work stems from the scientific collaboration between Cheikh Anta Diop University (Dakar, Senegal) and La Rochelle Université (La Rochelle, France). This study would not have been possible without the availability of the ERA5 wind field reanalysis, supported by the European Centre for Medium-Range Weather Forecasts (ECMWF), and the WWII model provided by the US NOAA. We would like to thank the various teams of the Laboratoire Mixte International d'Etude du Climat d'Afrique de l'Ouest (ECLAIRS) for sharing the MELAX buoy-observatory data off Dakar. Many thanks to the Centre de Suivi Ecologique de Dakar and the Fond Français pour l'Environnement Mondiale (FFEM) as part of the West Africa Coastal Area (WACA) Program for finding this research (Agreement N°CZZ2221.01. U.). Finally, we would like to thank the three anonymous reviewers for their constructive reviews, which improved this manuscript substantially.

Conflicts of Interest: The authors declare no conflict of interest.

References

1. Nicholls, R.J.; Wong, P.P.; Burkett, V.R.; Codignotto, J.O.; Hay, J.E.; McLean, R.F.; Ragoonaden, S.; Woodroffe, C.D. Coastal systems and lowlying areas. In *Climate Change 2007: Impacts, Adaptation and Vulnerability. Contribution of Working Group II to the Fourth Assessment Report of the Intergovernmental Panel on Climate Change*; Parry, M.L., Canziani, O.F., Palutikof, J.P., van der Linden, P.J., Hanson, C.E., Eds.; Cambridge University Press: Cambridge, UK, 2007; pp. 315–356.
2. Niang, N.A. Dynamique Socio-Environnementale et Gestion des Ressources Halieutiques des Régions Côtières du Sénégal: L'exemple de la Pêche Artisanale. Ph.D. Thesis, Université de Rouen, Rouen, France, 2009; 302p.
3. Bertin, X.; Bruneau, N.; Breihl, J.F.; Fortunato, A.B.; Karpytchev, M. Importance of wave ag and resonance in storm surges: The case of Xynthia, Bay of Biscay. *Ocean Model.* **2011**, *42*, 16–30. [[CrossRef](#)]
4. Sadio, M.; Anthony, E.J.; Diaw, A.T.; Dussouillez, P.; Fleury, J.T.; Kane, A.; Almar, R.; Kestenare, E. Shoreline Changes on the Wave-Influenced Senegal River Delta, West Africa: The Roles of Natural Processes and Human Interventions. *Water* **2017**, *9*, 357. [[CrossRef](#)]
5. WACA. *Un Littoral Résilient, des Communautés Résilientes, Rapport Annuel 2020*; Programme de Gestion du Littoral Ouest-Africain; World Bank Group: Washington, DC, USA, 2020; 80p.
6. Sadio, M.; Sakho, I.; Samou, S.M.; Gueye, A.; Diouf, M.B.; Deloffre, J. Multi-decadal dynamics of the Saloum River delta mouth in climate change context. *J. Afr. Earth Sci.* **2022**, *187*, 104451. [[CrossRef](#)]
7. Almar, R.; Kestenare, E.; Boucharel, J. On the key influence of remote climate variability from Tropical Cyclones, North and South Atlantic mid-latitude storms on the Senegalese coast (West Africa). *Environ. Res. Commun.* **2019**, *1*, 071001. [[CrossRef](#)]
8. Reguero, B.G.; Losada, I.; Mendez, F. A recent increase in global wave power as a consequence of oceanic warming. *Nat. Commun.* **2019**, *10*, 205. [[CrossRef](#)] [[PubMed](#)]
9. Sakho, I.; Sadio, M.; Camara, I.; Noblet, M.; Seck, A.; Saengsupavanich, C.; Ndour, A.; Diouf, M.B. Sea level rise and future shoreline changes along the sandy coast of Saloum Delta, Senegal. *Arab. J.* **2022**, *15*, 1547. [[CrossRef](#)]
10. Voudoukas, M.I.; Clarke, J.; Ranasinghe, R.; Reimann, L.; Khalaf, N.; Duong, T.M.; Simpson, N.P. African heritage sites threatened as sea-level rise accelerates. *Nat. Clim. Change* **2022**, *12*, 256–262. [[CrossRef](#)]
11. Cissé, C.O.T.; Almar, R.; Youm, J.P.M.; Jolicoeur, S.; Taveneau, A.; Sy, B.A.; Sakho, I.; Sow, B.A.; Dieng, H. Extreme Coastal Water Levels Evolution at Dakar (Senegal, West Africa). *Climate* **2023**, *11*, 6. [[CrossRef](#)]
12. Dodet, G.; Bertin, X.; Taborda, R. Wave climate variability in the north-east Atlantic Ocean over the last six decades. *Ocean Modell.* **2010**, *31*, 120–131. [[CrossRef](#)]
13. Reguero, B.G. Numerical Modeling of the Global Wave Climate Variability and Associated Environmental and Technological Risks. Ph.D. Thesis, Universidad de Cantabria, Spain, Santander, December 2012; pp. 65–123.
14. Bertin, X.; Prouteau, E.; Letetrel, C. A significant increase in wave height in the North Atlantic Ocean over the 20th century. *Glob. Planet. Change* **2013**, *106*, 77–83. [[CrossRef](#)]
15. Marshall, A.G.; Hemer, M.A.; Hendon, H.H.; McInnes, K.L. Southern annular mode impacts on global ocean surface waves. *Ocean Model.* **2018**, *129*, 58–74. [[CrossRef](#)]
16. Oliver, B.; Veitch, J.; Reason, C.J.C. Variability in high wave energy events around the southern African coast. *J. Geophys. Res. Ocean.* **2022**, *127*, e2021JC018255. [[CrossRef](#)]
17. Dahunsi, A.; Bonou, F.; Olusegun, D.; Ezinvi, B. A Spatio-Temporal Trend of Past and Future Extreme Wave Climates in the Gulf of Guinea Driven by Climate. *J. Mar. Sci. Eng.* **2022**, *10*, 1581. [[CrossRef](#)]
18. Osinowo, A.; Okogbue, E.; Eresanya, E.; Akande, S. Extreme significant wave height climate in the Gulf of Guinea. *Afr. J. Mar. Sci.* **2018**, *40*, 407–421. [[CrossRef](#)]
19. Young, I.; Zieger, S.; Babanin, A. Global Trends in Wind Speed and Wave Height. *Science* **2011**, *332*, 451–455. [[CrossRef](#)] [[PubMed](#)]
20. Timmermans, B.W.; Gommenginger, C.P.; Dodet, G.; Bidlot, J.R. Global wave height trends and variability from new multimission satellite altimeter products, reanalyses, and wave buoys. *Geophys. Res. Lett.* **2020**, *47*, e2019GL086880. [[CrossRef](#)]
21. Izaguirre, C.; Méndez, F.J.; Menéndez, M.; Losada, I.J. Global extreme wave height variability based on satellite data. *Geophys. Res. Lett.* **2011**, *38*, L10607. [[CrossRef](#)]

22. Kumar, P.; Min, S.; Weller, E.; Lee, H.; Wang, X. Influence of Climate Variability on Extreme Ocean Surface Wave Heights Assessed from ERA-Interim and ERA-20C. *J. Clim.* **2016**, *29*, 4031–4046. [[CrossRef](#)]
23. Kumar, P.; Kaur, S.; Weller, E.; Min, S.K. Influence of natural climate variability on the extreme ocean surface wave heights over the Indian Ocean. *J. Geophys. Res. Oceans* **2019**, *124*, 6176–6199. [[CrossRef](#)]
24. Patra, A.; Min, S.K.; Seong, M.G. Climate variability impacts on global extreme wave heights: Seasonal assessment using satellite data and ERA5 reanalysis. *J. Geophys. Res. Oceans* **2020**, *125*, e2020JC016754. [[CrossRef](#)]
25. Cassou, C.; Cherchi, A.; Kosaka, Y. IPCC. Annex IV: Modes of Variability. In *Climate Change 2021: The Physical Science Basis. Contribution of Working Group I to the Sixth Assessment Report of the Intergovernmental Panel on Climate Change*; Masson-Delmotte, V., Zhai, P., Pirani, A., Connors, S.L., Péan, C., Berger, S., Caud, N., Chen, Y., Goldfarb, L., Gomis, M.I., Eds.; Cambridge University Press: Cambridge, UK; New York, NY, USA, 2021; pp. 2153–2192. [[CrossRef](#)]
26. Bacon, S.; Carter, D.J.T. A connection between mean wave height and atmospheric pressure gradient in the North Atlantic Int. *J. Climatol.* **1993**, *13*, 423–436. [[CrossRef](#)]
27. Hurrell, J.W. Decadal trends in the North Atlantic Oscillation: Regional temperatures and precipitation. *Science* **1995**, *269*, 676–679. [[CrossRef](#)] [[PubMed](#)]
28. Kushnir, Y.; Cardone, V.J.; Greenwood, J.G.; Cane, M.A. The recent increase in North Atlantic Wave Heights. *J. Clim.* **1997**, *10*, 2107–2113. [[CrossRef](#)]
29. Woolf, D.K.; Cotton, P.D.; Challenor, P.G. Variability and predictability of the North Atlantic wave climate. *J. Geophys. Res.* **2002**, *107*, 3145. [[CrossRef](#)]
30. Hurrell, J.W.; Kushnir, Y.; Ottersen, G.; Visbeck, M. An overview of the North Atlantic oscillation. *Geophys. Monogr. Am. Geophys. Union* **2003**, *134*, 1–36.
31. Castelle, B.; Dodet, G.; Masselink, G.; Scott, T. Increased winter-mean wave height, variability, and periodicity in the Northeast Atlantic over 1949–2017. *Geophys. Res. Lett.* **2018**, *45*, 3586–3596. [[CrossRef](#)]
32. Morales-Márquez, V.; Orfila, A.; Simarro, G.; Marcos, M. Extreme waves and climatic patterns of variability in the eastern North Atlantic and Mediterranean basins. *Ocean Sci.* **2020**, *16*, 1385–1398. [[CrossRef](#)]
33. Hochet, A.; Dodet, G.; Ardhuin, F.; Hemer, M.; Young, I. Sea State Decadal Variability in the North Atlantic: A Review. *Climate* **2021**, *9*, 173. [[CrossRef](#)]
34. Marshall, G.J. Trends in the Southern Annular Mode from observations and reanalyses. *J. Clim.* **2003**, *16*, 4134–4143. [[CrossRef](#)]
35. Hemer, M.; Chruch, J.A.; Hunter, J.R. Variability and trends in the directional wave climate of the Southern Hemisphere. *Int. J. Climatol.* **2010**, *30*, 475–491. [[CrossRef](#)]
36. Hemer, M.; Fan, Y.; Mori, N.; Semedo, A.; Wang, X. Projected changes in wave climate from a multi-model ensemble. *Nat. Clim. Change* **2013**, *3*, 471–476.
37. Barnard, P.; Short, A.; Harley, M.; Splinter, K.D.; Vitousek, S.; Turner, I.L.; Allan, J.; Banno, M.; Bryan, K.R.; Doria, A.; et al. Coastal vulnerability across the Pacific dominated by El Niño/Southern Oscillation. *Nat. Geosci.* **2015**, *8*, 801–807. [[CrossRef](#)]
38. Izaguirre, C.; Mendez, F.J.; Menedez, M.; Luceno, A.; Losada, I.J. Extreme wave climate variability in Southern Europe using satellite data. *J. Geophys. Res.* **2010**, *115*, C04009. [[CrossRef](#)]
39. Shimura, T.; Mori, N.; Mase, H. Ocean Waves and Teleconnection Patterns in the Northern Hemisphere. *J. Clim.* **2013**, *26*, 8654–8670. [[CrossRef](#)]
40. Martínez-Asensio, A.; Tsimplis, M.N.; Marcos, M.; Feng, X.; Gomis, D.; Jordà, G.; Josey, S.A. Response of the North Atlantic wave climate to atmospheric modes of variability. *Int. J. Climatol.* **2016**, *36*, 1210–1225. [[CrossRef](#)]
41. Castelle, B.; Dodet, G.; Masselink, G.; Scott, T. A new climate index controlling winter wave activity along the Atlantic coast of Europe: The West Europe Pressure Anomaly. *Geophys. Res. Lett.* **2017**, *44*, 1384–1392. [[CrossRef](#)]
42. Almar, R.; Kestenare, E.; Reyns, J.; Jouanno, J.; Anthony, E.J.; Laibi, R.; Hemer, M.; Du Penhoat, Y.; Ranasinghe, R. Response of the Bight of Benin (Gulf of Guinea, West Africa) coastline to anthropogenic and natural forcing, Part1: Wave climate variability and impacts on the longshore sediment transport. *Cont. Shelf Res.* **2015**, *110*, 48–59. [[CrossRef](#)]
43. Dee, D.P.; Uppala, S.M.; Simmons, A.J.; Berrisford, P.; Poli, P.; Kobayashi, S.; Andrae, U.; Balmaseda, M.A.; Balsamo, G.; Bauer, P.; et al. The ERA-Interim reanalysis: Configuration and performance of the data assimilation system. *Q. J. R. Meteorol. Soc.* **2011**, *137*, 553–597. [[CrossRef](#)]
44. Winant, C.D.; Dorman, C.E.; Friehe, C.A.; Beardsley, R.C. The marine layer off northern California: An example of supercritical channel flow. *J. Atmos. Sci.* **1988**, *45*, 3588–3605. [[CrossRef](#)]
45. Colosi, L.V.; Villas Bôas, A.B.; Gille, S.T. The seasonal cycle of significant wave height in the ocean: Local versus remote forcing. *J. Geophys. Res. Oceans* **2021**, *126*, e2021JC017198. [[CrossRef](#)]
46. Diaw, A.T. Morphométrie du littoral sénégalais et gambien. *Notes Afr. Dakar* **1984**, *183*, 58–63.
47. CSE. *Rapport Sur l'état de L'Environnement au Sénégal, Edition 2005*; Ministère de l'Environnement et de la Protection de la Nature: Dakar, Senegal, 2005; 231p.
48. Niang, D.I. L'érosion Sur la Petite Côte du Sénégal à Partir de L'Exemple de Rufisque: Passé-Présent-Futur. Ph.D. Thesis, Université D'Angers, Angers, France, 1995; 317p.
49. Guilcher, A.; Nicholas, J.P. Observation sur la Langue de Barbarie et les bras du Sénégal aux environs de Saint-Louis. *Bull. D'inf. Com. Océanogr. Etudes Côtières* **1954**, *6*, 227–242. (In French)

50. Tolman, H.L. *User Manual and System Documentation of WAVEWATCH-III, Version 1.15*; NOAA/NWS/NCEP/OMB Technical Note 151; US Department of Commerce: Washington, DC, USA, 1997; 97p.
51. Tolman, H.L. *User Manual and System Documentation of WAVEWATCH-III, Version 1.18*; NOAA/NWS/NCEP/OMB Technical Note 166; US Department of Commerce: Washington, DC, USA, 1999; 110p.
52. Tolman, H.L. *User Manual and System Documentation of WAVEWATCH III, Version 3.14*; NOAA/NWS/NCEP/MMAB Technical Note 276; US Department of Commerce: Washington, DC, USA, 2009; 194p.
53. Wamdi Group. The WAM model—A third generation ocean wave prediction model. *J. Phys. Oceanogr.* **1988**, *18*, 1775–1810. [[CrossRef](#)]
54. Komen, G.J.; Cavaleri, L.; Donelan, M.; Hasselmann, K.; Hasselmann, S.; Janssen, P.A.E.M. *Dynamic and Modelling of Ocean Waves*; Cambridge University Press: Cambridge, UK, 1994; 532p.
55. Bidlot, J.R.; Holt, M.W. *Verification of Operational Global and Regional Wave Forecasting Systems Against Measurements from Moored Buoys*; JCOMM Technical Report 30; WMO & IOC: Geneva, Switzerland, 2006. [[CrossRef](#)]
56. Yanenko, N.N. *The Method of Fractional Steps, the Solution of Problems of Mathematical Physics in Several Variables*; Springer: Berlin/Heidelberg, Germany, 1971. [[CrossRef](#)]
57. Tolman, H.L.; Booij, N. Modeling wind waves using wavenumber direction spectra and a variable wavenumber grid. *Glob. Atmos. Ocean Syst.* **1998**, *6*, 295–309.
58. WaveWatch III R© Development Group. *User Manual and System Documentation of WAVEWATCH III, Version 6.07*; US Department of Commerce: Washington, DC, USA, 2019.
59. GEBCO. 2019. Available online: <https://download.gebco.net/> (accessed on 1 October 2020).
60. Hersbach, H.; Bell, B.; Berrisford, P.; Hirahara, S.; Horányi, A.; Muñoz-Sabater, J.; Nicolas, J.; Peubey, C.; Radu, R.; Schepers, D.; et al. The ERA5 global reanalysis. *Q. J. R. Meteorol. Soc.* **2020**, *146*, 1999–2049. [[CrossRef](#)]
61. Alday, M.; Ardhuin, F.; Accensi, M.; Dodet, G. A global wave parameter database for geophysical applications. Part 3: Improved forcing and spectral resolution. *Ocean. Model.* **2021**, *166*, 101848. [[CrossRef](#)]
62. Pineau-Guillou, L.; Ardhuin, F.; Bouin, M.N.; Redelsperger, J.L.; Chapron, B.; Bidlot, J.; Quilfen, Y. Strong winds in a coupled wave-atmosphere model during a north Atlantic storm event: Evaluation against observations. *Q. J. R. Meteorol. Soc.* **2018**, *144*, 317–332. [[CrossRef](#)]
63. Benetazzo, A.; Barbariol, F.; Davison, S.; Sclavo, M.; Favaretto, C.; Mercogliano, P. Correction of ERA5 Wind for Regional Climate Projections of Sea Waves. *Water* **2022**, *14*, 1590. [[CrossRef](#)]
64. Campos, R.M.; Gramscianinov, C.B.; de Camargo, R.; da Silva Dias, P.L. Assessment and Calibration of ERA5 Severe Winds in the Atlantic Ocean Using Satellite Data. *Remote Sens.* **2022**, *14*, 4918. [[CrossRef](#)]
65. Hasselmann, S.; Hasselmann, K.; Allender, J.; Barnett, T. Computation and parameterizations of the nonlinear energy transfer in a gravity-wave spectrum. Part II: Parameterizations of the nonlinear energy transfer for application in wave models. *J. Phys. Oceanogr.* **1985**, *15*, 1378–1391. [[CrossRef](#)]
66. Goring, D.G.; Nikora, V.I. Despiking acoustic doppler velocimeter data. *J. Hydraul. Eng.* **2002**, *128*, 117–126. [[CrossRef](#)]
67. Comas-Bru, L.; Hernández, A. Reconciling North Atlantic climate modes: Revised monthly indices for the East Atlantic and the Scandinavian patterns beyond the 20th century. *Earth Syst. Sci. Data* **2018**, *10*, 2329–2344. [[CrossRef](#)]
68. Alday, M.; Ardhuin, F.; Dodet, G.; Accensi, M. Accuracy of numerical wave model results: Application to the Atlantic coasts of Europe. *Ocean Sci.* **2022**, *18*, 1665–1689. [[CrossRef](#)]
69. Reguero, B.G.; Méndez, F.J.; Losada, I.J. Variability of multivariate wave climate in Latin America and the Caribbean. *Glob. Planet. Change* **2013**, *100*, 70–84. [[CrossRef](#)]
70. Lavaud, L.; Bertin, X.; Martins, K.; Pezerat, M.; Coulombier, T.; Dausse, D. Wave dissipation and mean circulation on a shore platform under storm wave conditions. *J. Geophys. Res. Earth Surf.* **2022**, *127*, e2021JF006466. [[CrossRef](#)]
71. Guerin, K. Dynamics of the Sandy Coastline from Thiaroye to Bargny (Bay of Goree-Senegal). Master’s Thesis, University of Paris 1-Sorbonne-Panthéon, Paris, France, 2003; 198p.
72. Hemer, M.A. Historical trends in Southern Ocean storminess: Long-term variability of extreme wave heights at Cape Sorell, Tasmania. *Geophys. Res. Lett.* **2010**, *37*, L18601. [[CrossRef](#)]
73. Tracy, F.T.; Tracy, B.; Resio, D.T. *ERDC MSRC Resource*; Technical Report Fall 2006; US Army Corps of Engineers: Washington, DA, USA, 2006.
74. Bunney, C.C.; Saulter, A.; Palmer, T. *Reconstruction of Complex 2D Wave Spectra for Rapid Deployment of Nearshore Wave Models, in Marine Structures and Breakwaters*; Institute of Civil Engineers Publishing: London, UK, 2013.

Disclaimer/Publisher’s Note: The statements, opinions and data contained in all publications are solely those of the individual author(s) and contributor(s) and not of MDPI and/or the editor(s). MDPI and/or the editor(s) disclaim responsibility for any injury to people or property resulting from any ideas, methods, instructions or products referred to in the content.